coatings

MDPI

Article

The Influence of Thin Gold Electrodes on the High-Temperature Impedance of Oxide Glasses

Natalia Anna Wójcik * and Ryszard Jan Barczyński

Advanced Materials Center, Institute of Nanotechnology and Materials Engineering, Gdańsk University of Technology, 11/12 G. Narutowicza Street, 80-233 Gdańsk, Poland; ryszard.barczynski@pg.edu.pl
* Correspondence: natalia.wojcik@pg.edu.pl; Tel.: +48-583-486-606

Abstract: The influence of thin gold electrodes on the electrical measurements of glasses at high temperatures was studied using impedance spectroscopy. The impedance was measured several times over a wide frequency range from 10 mHz to 1 MHz and the temperature ranged from 213 to 673 K under air and nitrogen atmospheres. The results showed a drop in the conductivity of more than an order of magnitude at a temperature around 603 K during heating. An additional relaxation process was found at the low-frequency region. The occurred process was correlated with the thermal disintegration of the gold nano-layer used as an improvement in the electrical contact. The possible ambiguous interpretation of high-temperature impedance spectra was presented as a consequence of performing the electrical measurements only during heating or cooling while using unstable thin gold electrodes. Moreover, a possible solution to this problem was proposed.

Keywords: thin Au layers; thermal dissociation of Au thin film; impedance measurements; gold electrodes effect

Citation: Wójcik, N.A.; Barczyński, R.J. The Influence of Thin Gold Electrodes on the High-Temperature Impedance of Oxide Glasses. *Coatings* **2022**, *12*, 784. https://doi.org/10.3390/coatings12060784

Academic Editor: Narottam P. Bansal

Received: 17 May 2022
Accepted: 4 June 2022
Published: 6 June 2022

1. Introduction

The electrical properties of many different materials such as glasses, ceramics, ferrites, nanocomposites, and nanorods have been thoroughly and widely studied by the impedance spectroscopy technique [1–7]. The electrical measurements can be conducted over wide frequencies and temperature ranges as well as under different atmospheres. Usually, samples are polished on both sides and thin layers of metal are deposited as electrodes to improve the electrical contact [8,9]. The most popular metals, which serve as electrode materials, are silver [8,10–15], gold [15–19], and less often platinum [9]. Silver is sometimes applied in the form of a paste on the sample surfaces and is known to tend to agglomerate during being annealed in an air or oxygen atmosphere [20]. Moreover, silver can evaporate even at low (573–623 K) temperature [21] and silver ions are mobile in many materials, therefore, it should be used only for measurements at a low-temperature range [22,23]. The second often-used metal is gold, which has been applied for high-temperature measurements [24–27], even up to a temperature of 873 K [15]. However, the application of gold electrodes also has its limitations, which are often ignored.

The information on the thickness of the deposited gold layer or conditions used during deposition is usually omitted in the literature [15–17,28], being considered as a trivial matter [29]. Unfortunately, solid metallic films such as Au layers deposited on a substrate can be metastable or unstable in the as-deposited state and can undergo dewetting or agglomerate to form islands during heating to sufficiently high temperatures [30–32]. Interestingly, this process can be observed even significantly below the melting temperature of the film, moreover, it depends on the heating duration and rate [33]. The dissociation of thin Au film can be instant at higher temperatures or can take several hours at lower ones, which means that it has an activation character. For example, for 100 nm Au films deposited on the Al_2O_3 surface, it was found that it started to dissociate at 1130 K after 30 s and at 1020 K after ~4700 s [33]. On the other hand, impedance measurements can be

conducted for a long time at a specific temperature. Usually, a typical test conducted at a frequency range of 10 mHz to 1 MHz takes around 30 min for one selected temperature. Therefore, one should be aware of the processes that correlate with the Au electrodes when analyzing the impedance measurement results conducted at a high-temperature range.

This paper aimed to highlight the problem of the electrode effects on the electrical measurements at high temperatures. In the present work, we will show the effect of an unsuitable thickness of the deposited gold electrodes on the electrical results. The second problem discussed is the temperature limitation of using gold layers as an improvement in electrical contact. Moreover, the possible ambiguous interpretation of impedance spectra will be presented as a consequence of performing electrical measurements only during heating or cooling.

2. Materials and Methods

The electrical measurements were conducted on two exemplar oxide glass samples of different compositions. The first sample was silicate-based glass: $31.2Na_2O$-5.4BeO–$1.2Al_2O_3$–$62.1SiO_2$ in mol% (named 5BeNa). The second sample was phosphate-based glass: $9.4MgO$-$57.7P_2O_5$–$31.2CaO$-$1.7Al_2O_3$ in mol% (named 10 Mg). The detailed descriptions of the preparation technique and conditions applied during melting have been described in previous papers [19,34,35].

Complex impedance measurements were carried out in the frequency range from 10 mHz to 1 MHz and the temperature range of 213 K to 673 K, with an AC voltage of 1 V_{rms} using a Novocontrol Concept 40 broadband dielectric spectrometer (Novocontrol, Montabaur, Germany) at a constant voltage mode. The temperature step was selected as 10 K. The low-temperature measurements (213–473 K) were conducted in a nitrogen atmosphere. The high-temperature measurements (373–673 K) were carried out using a high-temperature Novotherm HT 1600 Controller (Novocontrol, Montabaur, Germany) under air and nitrogen atmospheres. Measurements were conducted for heating and cooling a few times in the low- and high-temperature ranges. The first sample of 5BeNa was measured seven times, as listed in Table 1. The second sample of 10 Mg was measured three times, as listed in Table 2. The measurements were conducted one after another. This means that first, the electrical properties of the 5BeNa sample were measured at a low-temperature range in a nitrogen atmosphere for cooling temperature. Next, the sample was placed in a high-temperature measuring chamber and tested in an air atmosphere for the cooling temperature. After that, it was placed once again in the low-temperature chamber and checked the same as the first time. Before the fourth measurement, the sample was polished and new gold electrodes were evaporated (a description of the electrode evaporation is given below). With the new electrodes, the fourth measurement was conducted under the same conditions as the first and third. The fifth measurement was conducted at high temperatures for heating and cooling in the nitrogen atmosphere. After that, the sample was measured twice again in the same chamber but under an air atmosphere. The IDs of the measurements suggest the number of measurements, low—LT or high-temperature—HT type and in the case of HT, also the atmosphere. The second sample of 10 Mg was studied only at high temperatures and an air atmosphere and for heating and cooling. The maximum temperature of the high-temperature measurements was selected to be lower than the glass transition temperature for both samples (T_g was found to be higher than 773 K) [34,35].

Table 1. The list of conditions used for the electrical measurements of the 5BeNa sample.

ID	Temperature Range	Atmosphere	Heating or Cooling Temperature	The Thickness of Gold Electrodes
1st m LT	Low 213–473 K	Nitrogen	Cooling	25 nm
2nd m HT air	High 373–673 K	Air	Cooling	25 nm
3rd m LT	Low 213–473 K	Nitrogen	Cooling	25 nm
After the above three tests, both sides of the sample were polished to remove a thin layer of surface and new gold electrodes were deposited.				
4th m LT	Low 213–473 K	Nitrogen	Cooling	25 nm
5th m HT N_2	High 373–673 K	Nitrogen	Heating and cooling	25 nm
6th m HT air	High 373–673 K	Air	Heating and cooling	25 nm
7th m HT air	High 373–673 K	Air	Heating and cooling	25 nm

Table 2. The list of conditions used for the electrical measurements of the 10 Mg sample.

ID	Temperature Range	Atmosphere	Heating or Cooling Process	The Thickness of Gold Electrodes
1st m HT	High 373–523 K	Air	Heating and cooling	>700 nm
2nd m HT	High 373–623 K	Air	Heating and cooling	>700 nm
After the 2nd test, both sides of the sample were polished to remove a thin layer of the surface.				
3rd m HT	High 373–673 K	Air	Heating and cooling	Without electrodes

For the electrical measurements, gold electrodes with different thicknesses were deposited at the polished plane surfaces of the circular samples. First, for the 5BeNa sample, a gold film with a thickness of 25 nm was deposited using a precise plasma sputtering coating device (Leica EM SCD050 (Leica, Vienna, Austria)) with control of the film thickness. Second, for the 10 Mg sample, thick gold electrodes were deposited using a resistance sputtering coating machine without control of the layer thickness. The approximate thickness of the thick electrodes was estimated to be more than 700 nm with the use of a scanning electron microscope (SEM), FEI Company Quanta FEG250 (Brno-Černovice, Czech Republic). More SEM observations of the surfaces of the samples were conducted after impedance measurements at high temperatures. Measurements were conducted using a 10 kV beam accelerating voltage with a SE-ETD detector (secondary electron—Everhart-Thornley detector) working in high vacuum mode (pressure 10^{-4} Pa).

3. Results and Discussion

This work was divided into three parts. In the first part, the authors present the problem, which can occur during a typical analysis of electrical properties conducted at a high-temperature range with the use of gold electrodes deposited on the surfaces of the samples. In the second part, the reason for the observed discrepancies in the results is given, and in the last part, possible solutions are proposed.

3.1. Presentation of the Problem

3.1.1. Conductivity Spectra for 5BeNa

First, the electrical impedance of the 5BeNa glass was checked at a low-temperature range from 213 to 473 K, under a nitrogen atmosphere, during a cooling process (1st m LT in Table 1). Figure 1a presents the frequency dependence of the real part of conductivity σ′ at different temperatures for this test. Usually, the conductivity spectra of many glasses can be divided into two parts: the frequency-independent DC conductivity (σ_{DC}) and the AC conductivity, which increases with frequency [36]. Typically, the frequency range of the DC plateau increases with the temperature. However, the studied glass additionally

showed a frequency-dependent conductivity part visible at frequencies lower than 1 Hz and at temperatures above 413 K, which can be correlated with the electrode effects and is often observed for ionic conductors [19]. So-called "electrode effects" are usually caused by double-layer formation at the electrode boundary due to the partially or fully blocking electrodes. Such a layer behaves in a similar way as a capacitor of large capacitance and contributes to the impedance results. Figure 1b displays the conductivity spectra obtained during the second measurement of the same 5BeNa sample conducted at high temperatures of 373–673 K, under an air atmosphere, and also during the cooling process (2nd m HT air). Some relaxation processes can be observed at temperatures below 513 K for the AC part, while for higher temperatures, DC plateau and electrode effects dominate. The low-temperature relaxation processes cannot be correlated with relieving the residual internal stresses introduced during the manufacturing process because the glass was annealed under air at a temperature of 673 K. Interestingly, the deposited gold electrodes changed color after the high-temperature test to a darker color. Therefore, two hypotheses of the origin of the observed relaxation process were made: (1) a conduction process activated in oxygen and (2) a process correlated with the electrodes' effects (above-mentioned). To check both options, a set of tests was conducted. The third measurement, conducted under the same conditions as the first, was carried out to check whether the relaxation process found for the 2nd m HT air (at temperature 373–513 K) will be observed for a nitrogen atmosphere. Figure 1c presents the conductivity spectra for the 3rd m LT. The relaxation process is visible. This result supports the idea that during a heating process up to the temperature of 673 K under air, some changes took place in the junction between the glass surface and the deposited electrodes, which influenced the sample's electrical properties.

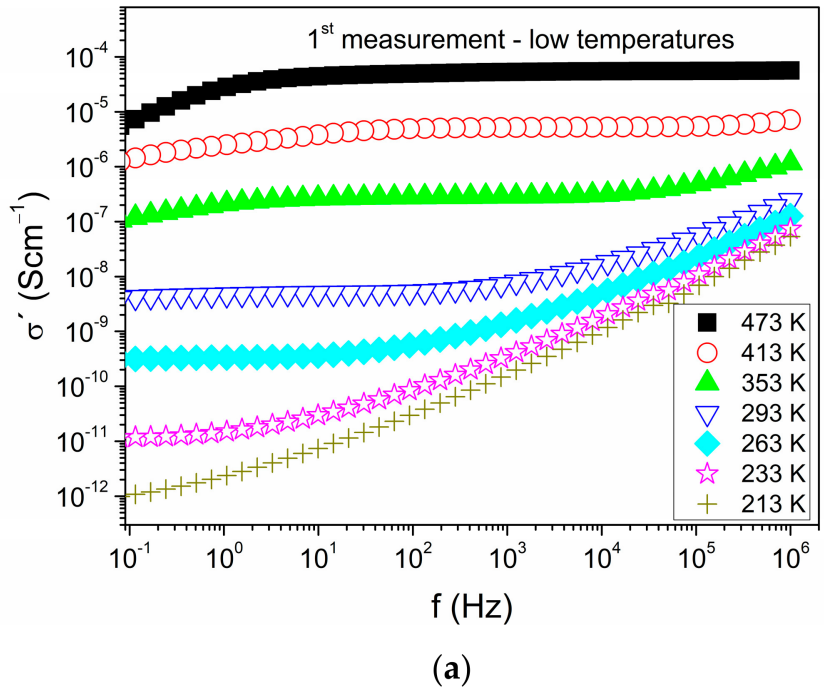

Figure 1. *Cont.*

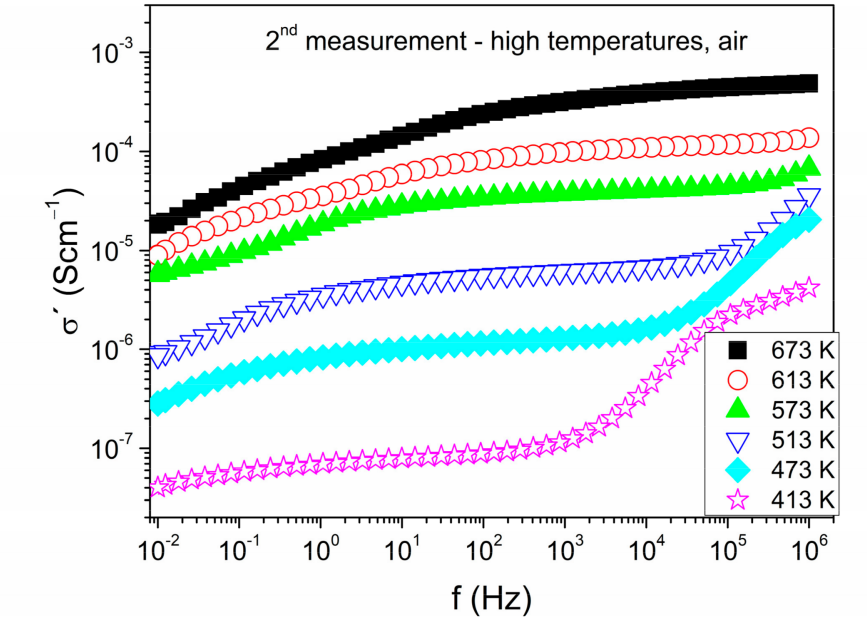

(**b**)

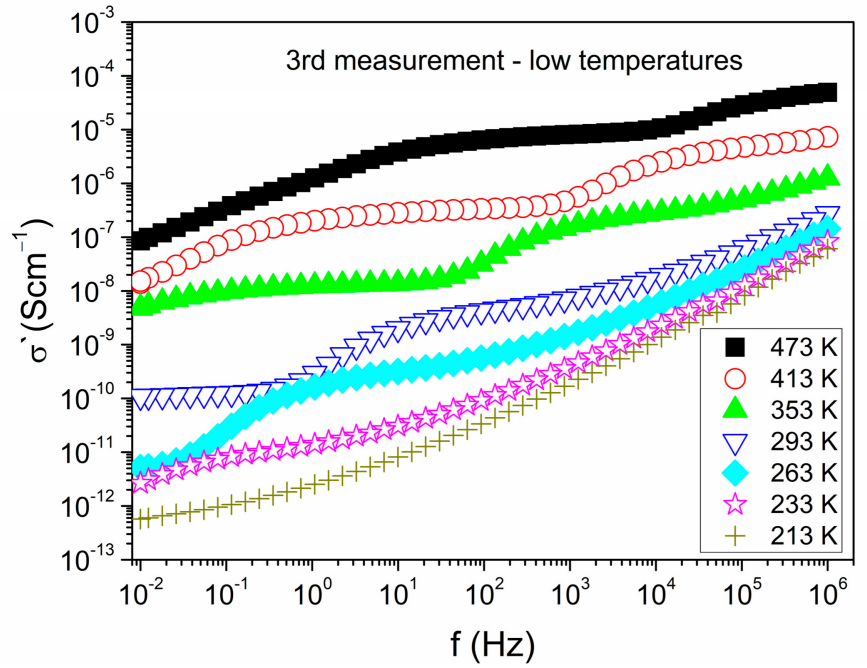

(**c**)

Figure 1. The frequency dependence of the real part of the AC conductivity at different temperatures: (**a**) First measurement at low temperatures, (**b**) second measurement at high temperatures and air atmosphere, and (**c**) third measurement at low temperatures. All measurements were conducted during cooling.

3.1.2. The Evolution of Conductivity Behavior during Subsequent Measurements for the 5BeNa Sample

To check whether the conductivity evolution was due to the surface effects and whether it was reproducible, both sides of the sample were polished to remove a thin layer of the surface and new gold electrodes were evaporated. The fourth m LT measurement was

conducted once again at a low-temperature range under a nitrogen atmosphere and no relaxation process was observed. Figure 2a shows the comparison of the real part of the AC conductivity for different measurements as a function of the temperature measured at a frequency of 100 Hz. The conductivity values obtained during the 4th m LT test were found to be the same as during the 1st m LT test. While comparing them with the ones obtained for the 2nd m HT air and 3rd m LT tests, the decrease in conductivity was observed for temperatures above 300 K due to the appearance of an additional relaxation process. These results indicate that the detected process was associated with the glass surface or gold electrode behavior. The fifth measurement (5th m HT N_2) was conducted at high temperatures under a nitrogen atmosphere to check whether this process is correlated with an oxidation process or is oxygen-independent. This test was conducted twice, during heating and cooling. It can be seen that during heating, the conductivity values obtained for the fifth m HT N_2 were approximately the same as for the first and fourth m LT. The trend in the increase in the conductivity with temperature was preserved up to 603 K, and above this temperature, the conductivity started to decrease. The drop was found to be more than one order of magnitude for the increase in temperature of 70 K.

The above results show that a process responsible for anomalous changes in resistivity begins at around a temperature of 603 K. The conductivity values in nitrogen (5th m HT N_2) were close to the ones measured in air (2nd m HT air and 3rd m LT), however, some discrepancies were noticeable. This may suggest that the studied process only slightly depends on the atmosphere.

The next two measurements 6th and 7th were conducted under air and during heating and cooling. The conductivity for heating under an air atmosphere (6th m HT air) showed higher values than for cooling in the 5th m HT N_2 test. Two distinct steps of decrease in the conductivity were observed at temperatures of 483 K and 573 K. During the 7th m HT air, there were still some discrepancies between the heating and cooling curves. We can conclude that the observed process between the glass surface and gold electrodes occurred continuously and caused changes in the measured resistance of the sample.

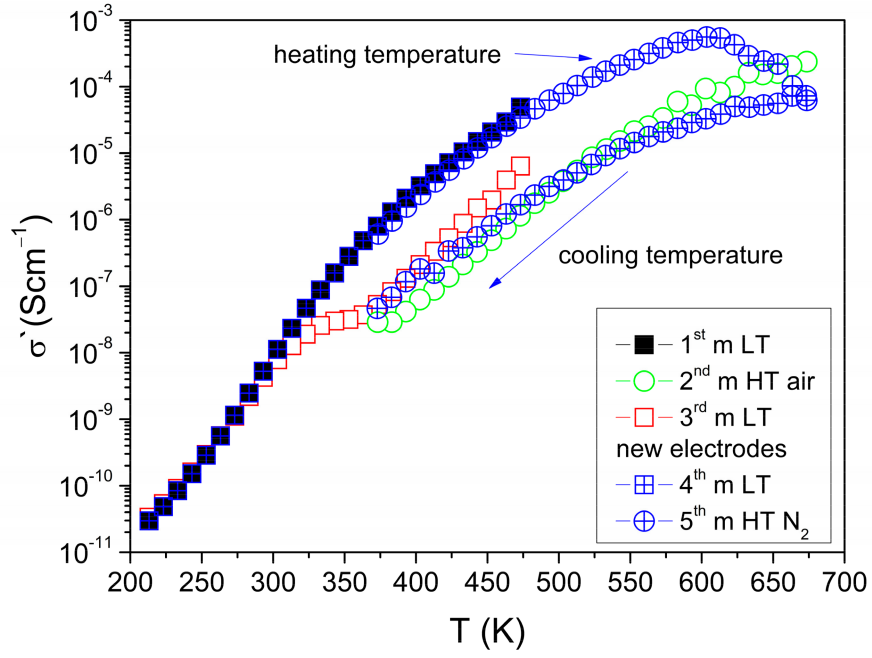

(**a**)

Figure 2. *Cont.*

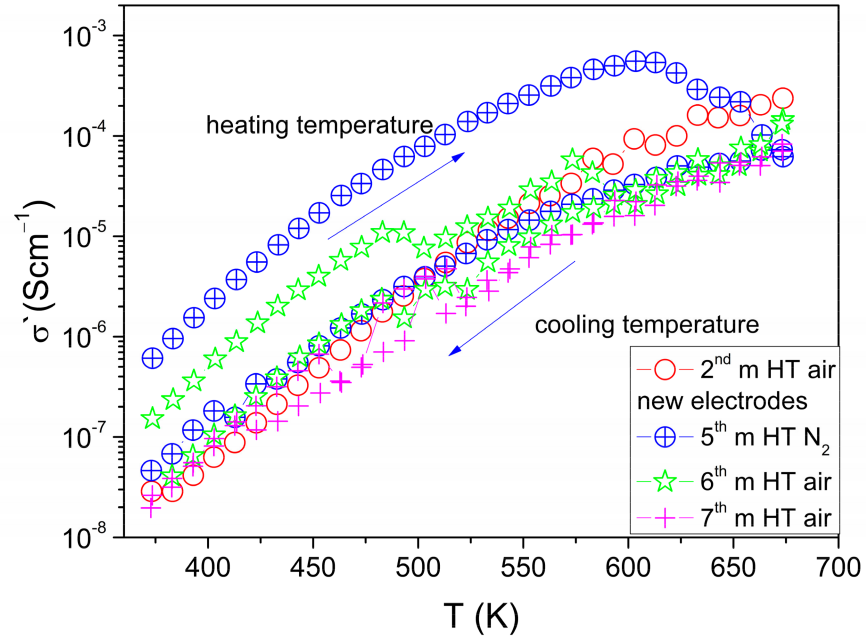

(**b**)

Figure 2. The temperature dependence of the real part of the AC conductivity at a frequency of 100 Hz for (**a**) 1st, 2nd, 3rd, 4th, and 5th tests and (**b**) 2nd, 5th, 6th, and 7th tests.

3.1.3. The Uncertainty in the Interpretation of Impedance Data

Routinely, electrical impedance is measured only during heating or cooling, usually without mentioning which one. In this section, we want to show that such an incomplete analysis of impedance spectra may be misleading.

Figure 3 shows the exemplar Nyquist plots conducted for all seven measurements for the 5BeNa sample. Such plots are usually used to illustrate and compare the impedance data. In Figure 3a, the comparison of Nyquist plots is shown for the 1st m LT, 2nd m HT air, and 3rd m LT tests. Significant evolution of spectra was visible. For the 1st m LT test, only one full semicircle appeared at a temperature of 383 K, which correlated with the relaxation process, however, the beginning of the second relaxation process was also found. The Nyquist plots of the sample measured during the 2nd m HT air and 3rd m LT consisted of two relaxation processes and the beginning of the third one. The temperature of 383 K was selected because it overlapped for both the low- and high-temperature measurements. After heating above the temperature of 673 K and under air, the additional relaxation process occurred. An increase in the total resistivity compared with the one obtained during the 1st m LT was also observed. Figure 3b displays the comparison of Nyquist plots for the sample measured during the initial 1st m LT measurement, and after preparing the new electrodes, the 4th m LT, and heating of the 5th m HT N_2 tests. All three curves were in fairly good agreement.

Figure 3c presents a comparison of the Nyquist plots obtained during cooling after achieving a high-temperature region: for the 2nd m HT air, 5th m HT N_2, 6th m HT air, and 7th m HT air tests. A shift in total resistivity was noticed. The lowest total resistivity was found for measurements under a N_2 atmosphere (black color in Figure 3c) and it increased for the measurements under air. However, the first semicircle observed at the high-frequency range overlapped for all four measurements (see insert in Figure 3c). The comparison of Nyquist plots obtained during heating and cooling temperature for the 6th m HT air and 7th m HT air tests are shown in Figure 3d. It can be seen that the resistivity of the sample further increased upon subsequent cycles, but changes were much smaller. Similar observations of discrepancies in the impedance behavior were also found for different temperatures.

The Nyquist plots of the 5BeNa sample obtained during the seven measurements were analyzed with the use of the Cole–Cole empirical relation [37]:

$$Z^* = R(1 + j\omega\tau)^{\alpha-1} \quad (1)$$

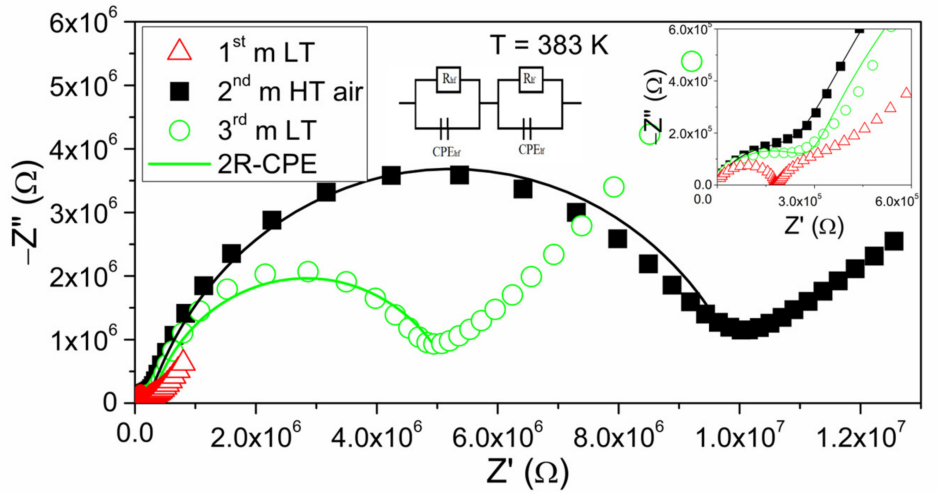

(**a**)

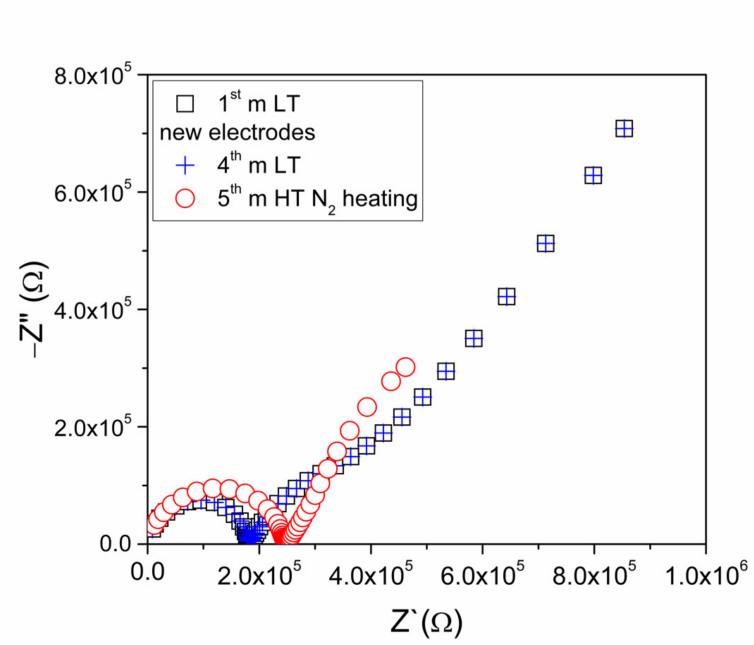

(**b**)

Figure 3. *Cont.*

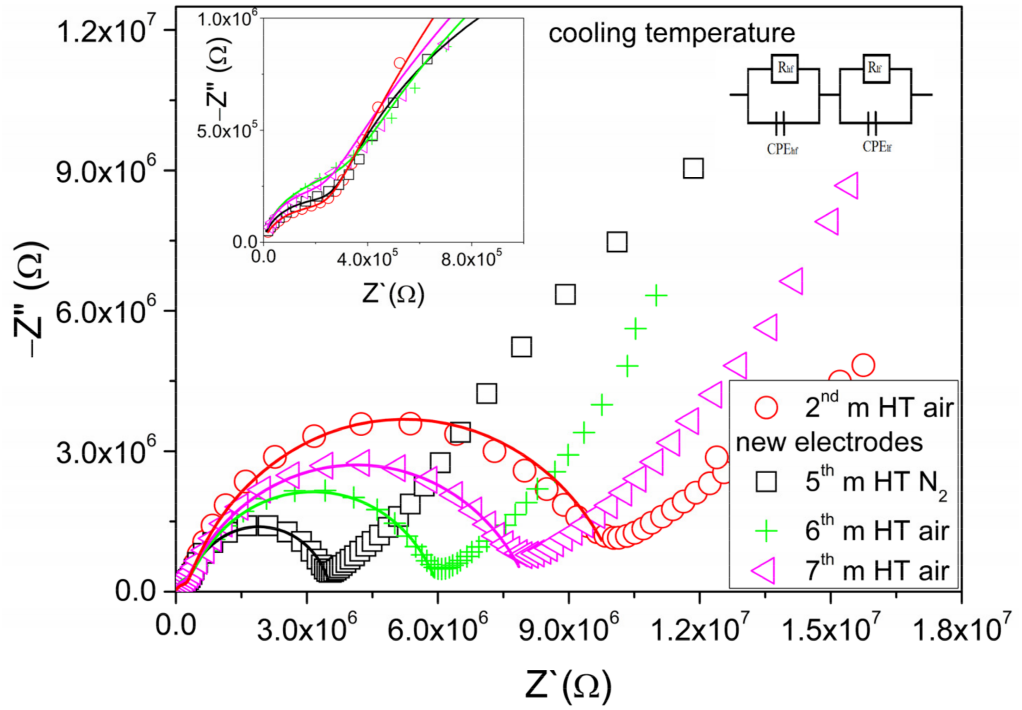

(**c**)

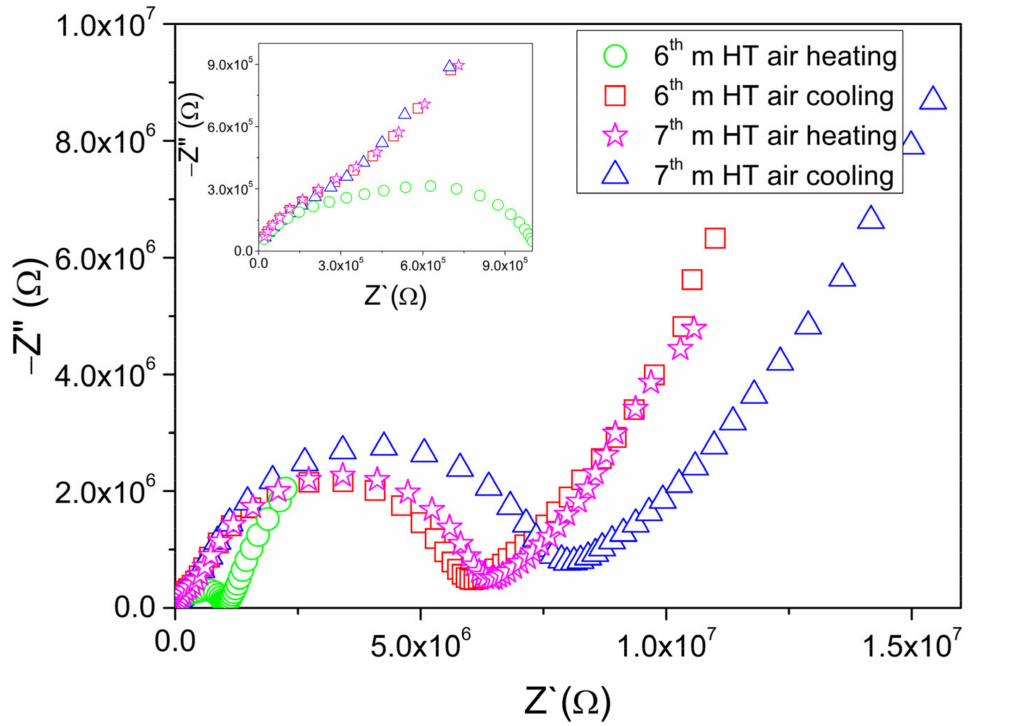

(**d**)

Figure 3. The comparison of Nyquist plots at an exemplar temperature of 383 K for: (**a**) 1st m LT, 2nd m HT air, 3rd m LT, (**b**) 1st m LT, 4th m LT, 5th m HT N_2 heating, (**c**) 2nd m HT air, 5th m HT N_2, 6th m HT, 7th m HT all during cooling and (**d**) 6th m HT air and 7th m HT air during cooling and heating. Inserts in the figures show the magnification of the high-frequency process. Lines are the results of fitting the 2R-CPE relation.

In this expression, a resistivity and a constant phase (CPE) element are connected in parallel and Z* is the complex impedance, R is the equivalent resistivity, τ is the mean dielectric relaxation time, ω is an angular frequency, and α is a parameter that describes the width of the relaxation time distribution. The equivalent circuit used for fitting the results consists of one or two circuits described by the Cole–Cole relations connected in series (shown in Figure 3a,c). The lines in Figure 3 show the exemplar results of the fitting. This is in good agreement with the experimental results. The impedance analysis was conducted in the full possible temperature range. The highest possible temperature at which the fitting was possible and provided reasonable results was 473 K. Above, the nonlinearity correlated with the electrode effects (like double-layer formation) was not negligible and the correct estimation of the two relaxation processes was impossible. As can be seen in Nyquist plots (Figure 3), two relaxation processes highly overlapped in most of the cases, therefore, it is hard to define the boundary frequency that separates the low- and high-frequency regions. However, the obtained relaxation times were 100 up to 1000 times different between the high- and low-frequency relaxation processes. The resistivity values estimated from fitting were used to calculate the equivalent conductance of the observed relaxation processes. The conductance was estimated based on the sample dimensions. Figure 4 displays the conductance values connected with the relaxation processes that occurred at high- and low-frequency regions calculated for cooling temperature. They obey the Arrhenius law, described by the expression:

$$\sigma_{DC}T = \sigma_0 \exp(\frac{-E_A}{kT}) \quad (2)$$

where σ_0 is the conductivity pre-exponential factor; E_A is the activation energy; and k is the Boltzman's constant. The activation energy is calculated based on the linear fitting of conductance values multiplied by the temperature and presented as a function of reciprocal temperature $ln(\sigma T) = f(T^{-1})$. This dependence showed a linear behavior in a wide temperature range, which is typical for ionic conduction. The linear fitting showed good agreement with the experimental data. In this paper, the conductance was presented as a function of $1000T^{-1}$ as is customary to facilitate the analysis of conductivity values. The values of E_A estimated from the fitting with Equation (2) are listed in Table 3. The equivalent conductance estimated for the high-frequency relaxation process was similar for all seven measurements. However, the activation energy calculated for this process varied between 0.52 and 0.7 eV, which is a big discrepancy. Only for the 1st m LT and 4th m LT tests were the results the same. For the second relaxation process, which occurred in the low-frequency region, the discrepancies between the conductance values were larger while the activation energy values were in the lower variances. The second relaxation process, which appeared only after heating above 603 K, was thermally activated and may be due to the interaction between the sample glass surface and electrodes. As it is well known that 5BeNa glass is a typical ionic conductor, we can assume that the higher frequency relaxation process is due to sodium ion hopping, while the beginning of the third process is correlated with the accumulation of sodium ions at the electrodes [12]. However, if we only analyze the results during cooling, the second relaxation that occurred at the low-frequency region could be wrongly interpreted, for example, as an additional conduction process inside the sample. Moreover, it can be seen that the differences between the results upon cooling and heating were large, which may be misleading.

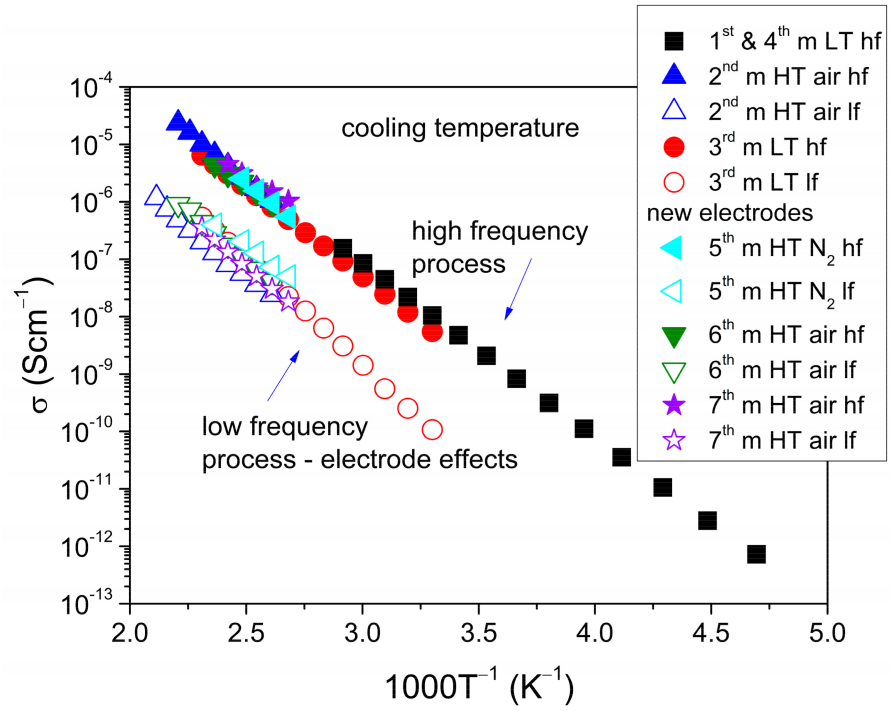

Figure 4. The conductivity versus reciprocal temperature for the relaxation processes was estimated from Figure 3.

Table 3. The activation energy values for the relaxation processes observed in the Nyquist plots and estimated from Figure 4 and relation (2).

	E_A (eV) ± 2%						
					New Electrodes		
Process	**1st m LT**	**2nd m HT Air**	**3rd m LT**	**4th m LT**	**5th m HT N_2**	**6th m HT Air**	**7th m HT Air**
High frequency	0.62	0.70	0.65	0.62	0.69	0.57	0.52
Low frequency	-	0.71	0.77	-	0.65	0.71	0.72

3.2. The Possible Origin of Impedance Evolution

There are a few possible explanations for the process that proceeded on the sample surfaces during heating. One of them is the formation of Si-Au eutectics, which is known to take part around a temperature of 643 K [38,39]. However, a similar observation was made for phosphate glass, which does not contain silicon (see Section 3.3). The second possibility is a disruption of the Au thin layer continuity. As described earlier, the disruption can occur as a result of Au film disintegration due to dewetting or agglomeration into the form of islands [30–32]. This process was observed for 20 nm Au film deposited on the Al_2O_3 substrate at a temperature of 810 K after 30 s and at a temperature of 760 K, but after a long time of approximately 4500 s [33].

The topography of samples was observed with the use of SEM. The exemplar micrographs of the 5BeNa sample surfaces after the impedance measurements at high temperatures under air are presented in Figure 5, in two different magnifications. It can be seen that the gold electrode layer became discontinuous after heating above 673 K. It confirms that the thermal disintegration of thin gold electrodes occurred. This can explain the high increase in the sample resistance. The thickness of the evaporated gold electrodes was 25 nm and it was thick enough to obtain good electrical contact. However, the temperature at which the resistance increased was significantly lower than the one observed for the dissociation of the 20 nm Au layer [33]. This shift may have been caused by the different

heating rates and time of measurement. Both had a high effect on the temperature of the Au film thermal disintegration. The second relaxation process, which was found in the impedance plots at the low-frequency region, accompanied the thermal disintegration process of the gold nano-layer.

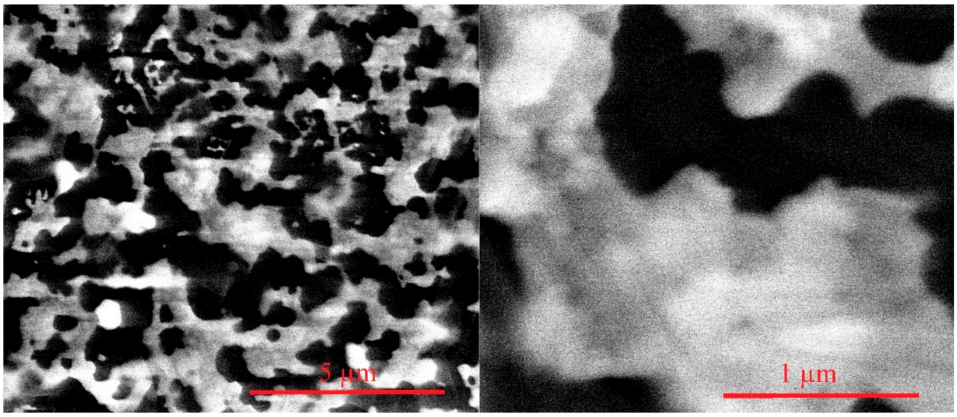

Figure 5. The SEM micrographs for the 5BeNa sample after the impedance measurements (gold electrodes, 25 nm).

3.3. Avoiding Effects of Electrode Disintegration

Usually, researchers are interested in the achievement of good electrical contact. Thus far, we have shown that a thin gold layer with a thickness of 25 nm is enough to obtain good electrical contact. However, as thermal disintegration is an obvious process for the Au nanosize layer, we decided to check the observed process for the thick electrodes customarily used during electrical measurements. For this purpose, thick gold electrodes were deposited on a 10 Mg sample in a vacuum using a resistance sputtering coating machine. A long time of deposition was used to obtain thick gold layers. The phosphate glass sample was selected to prevent the possibility of the formation of Si-Au eutectics. The approximate thickness of the electrodes was found to be higher than 700 nm.

Three impedance measurements were conducted at high temperatures under an air atmosphere and the results are presented in Figure 6. The first and second measurements were conducted with thick gold electrodes and it can be seen that during heating up to 523 K, the results were in good agreement. However, heating above a temperature of 623 K caused a decrease in the conductivity values, similar to the 5BeNa sample with thin electrodes (see Figure 2). The temperature of the conductivity jump was found to be slightly higher at 623 K. The difference in impedance values measured for the heating and cooling temperatures is also visible in the Nyquist plots in Figure 6b. The additional second relaxation process was visible (red crosses) for the 2nd m HT test for the cooling temperature. Figure 7 presents the SEM micrograph of the 10 Mg sample after the 2nd m HT test. It can be seen that the thermal disintegration of the gold electrodes also occurred. However, the disintegration was less pronounced than for the 25 nm Au layer, which was expected. Unfortunately, even a little disintegration still highly affects the electrical measurements.

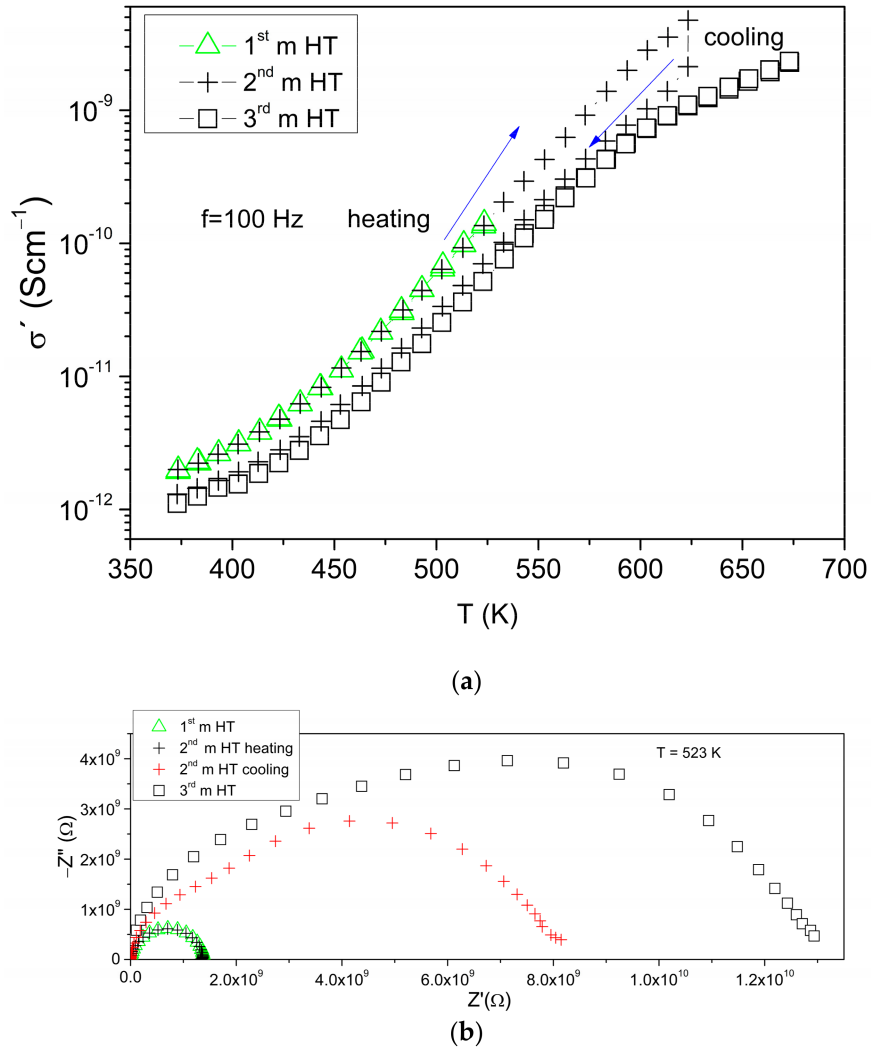

Figure 6. (**a**) The temperature dependence of the real part of the AC conductivity at a frequency of 100 Hz for: 1st m HT, 2nd m HT, and 3rd m HT measurements conducted under an air atmosphere for the 10 Mg sample. (**b**) The comparison of Nyquist plots at an exemplar temperature of 523 K for the 1st m HT, 2nd m HT cooling and heating, and 3rd m HT measurements.

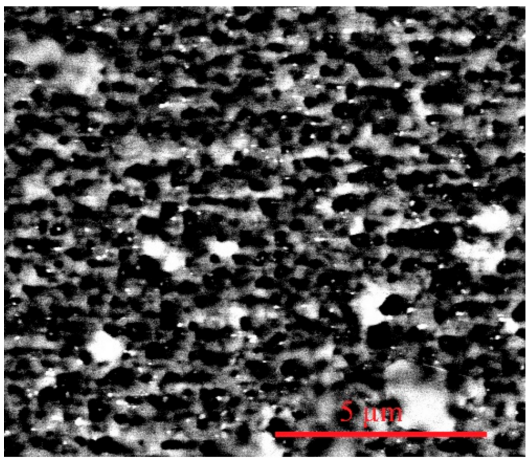

Figure 7. The SEM micrographs for the 10 Mg sample after the impedance measurements (gold electrodes > 700 nm).

One possible solution to prevent electrode influence is by performing measurements without evaporated layers and/or insulated (blocking) electrodes. Such measurements without gold electrodes are presented in Figure 6 (squares). The parameters of relaxation may be obtained by fitting to the equivalent model. The values of conductivity obtained by fitting were close to the ones with gold electrodes obtained during cooling. It was confirmed that the decrease in conductivity was due to the deterioration of electrical contact between the sample and equipment as a consequence of breaking the continuity of the gold layer. The impedance plot for the sample without gold layers also exhibited two relaxation processes. The second process was most probably due to the double layer effect connected with the accumulation of ions on electrodes. One advantage of measurements without deposited electrodes over measurements with deposited thick gold electrodes is that the found second relaxation process is thermally stable and can be easily subtracted from the total impedance. The thermal dissociation of Au film can even take several hours at lower temperatures [33], therefore, it can change during further measurements. To resolve the problem with the volatile process of the thermal disintegration of gold layers, there is the other more expensive possibility of using the platinum electrodes, which can be used at a higher temperature range than that of gold electrodes.

4. Conclusions

It was shown that using the thin gold layers as an improvement in the electrical contact during the high-temperature impedance measurements may cause difficulties in the interpretation of the obtained results. It can be recommended that the high-temperature measurements with deposited gold electrodes should be conducted only up to about 600 K. The thickness of the gold electrodes should be taken into account during the preparation of samples for the electrical measurements. The high-temperature measurements should be conducted for heating and cooling and both results should be considered.

To avoid problems with a volatile process of the thermal disintegration of gold layers, there is another possibility: performing electrical measurements without deposited electrodes and with insulated electrodes. Then, the second relaxation process can be addressed, for instance, the double layer effect, and can be subtracted from the total impedance.

Author Contributions: N.A.W.: conceptualization; data curation; formal analysis; investigation; methodology; project administration; resources; software; supervision; validation; visualization; roles/writing—original draft. R.J.B.: methodology; project administration; supervision; validation; writing—review & editing. All authors have read and agreed to the published version of the manuscript.

Funding: This research received no external funding.

Institutional Review Board Statement: Not applicable.

Informed Consent Statement: Not applicable.

Data Availability Statement: The data that support the findings of this study are available from the corresponding author upon reasonable request.

Acknowledgments: We wish to thank Marcin Łapiński for the SEM measurements.

Conflicts of Interest: The authors declare no conflict of interest.

References

1. Sagar, T.V.; Rao, T.S.; Naidu, K.C.B. AC-electrical conductivity, magnetic susceptibility, dielectric modulus and impedance studies of sol-gel processed nano-NiMgZn ferrites. *Mater. Chem. Phys.* **2021**, *258*, 123902. [CrossRef]
2. Reddy, B.V.S.; Srinivas, K.; Kumar, N.S.; Naidu, K.C.B.; Ramesh, S. Nanorods like microstructure, photocatalytic activity and ac-electrical properties of (1−x) ($Al_{0.2}La_{0.8}TiO_3$) + (x) ($BaTiO_3$) (x = 0.2, 0.4, 0.6 & 0.8) nanocomposities. *Chem. Phys. Lett.* **2020**, *752*, 137552.
3. Assad, H.; Kharroubi, M. Dielectric studies and Cole-Cole plot analysis of Na_2O – (1−x) ZnO – xCoO – P_2O_5 glasses. *J. Non-Cryst. Solids* **2021**, *560*, 120721. [CrossRef]

4. Xi, J.; Xing, J.; Chen, H.; Zhang, F.; Chen, Q.; Zhang, W.; Zhu, J. Crystal structure and electrical properties of Li/Mn co-doped NBT-based Aurivillius-type ceramics. *J. Alloys Compd.* **2021**, *868*, 159216. [CrossRef]
5. Thirmal, C.; Ramarao, S.; Rao, L.S.; Murthy, V. Study of structural, dielectric and AC conductivity properties of $SrMoO_4$. *Mater. Res. Bull.* **2021**, *146*, 111618. [CrossRef]
6. Raghuram, N.; Rao, T.S.; Naidu, K.C.B. Chandra Babu Naidu, Electrical and impedance spectroscopy properties of hydrothermally synthesized $Ba_{0.2}Sr_{0.8-y}La_yFe_{12}O_{19}$ (y = 0.2–0.8) nanorods. *Ceram. Int.* **2019**, *46*, 5894–5906. [CrossRef]
7. Kumar, N.S.; Suvarna, R.P.; Reddy, K.R.K.; Babu, T.A.; Ramesh, S.; Reddy, B.V.S.; Manjunatha, H.; Naidu, K.C.B. Tetragonal structure and dielectric behavior of rare-earth substituted $La_{0.8}Co_{0.16-x}Eu_{0.04}Gd_xTiO_3$ (x = 0.04–0.16) nanorods. *Mater. Chem. Phys.* **2022**, *278*, 125598. [CrossRef]
8. Babu, N.R.; Valente, M.; Rao, N.N.; Graça, M.; Raju, G.N.; Piasecki, M.; Kityk, I.; Veeraiah, N. Low temperature dielectric dispersion and electrical conductivity studies on Fe_2O_3 mixed lithium yttrium silicate glasses. *J. Non-Cryst. Solids* **2012**, *358*, 3175–3186. [CrossRef]
9. Souissi, F.Z.; Ettoumi, H.; Barré, M.; Toumi, M. Preparation and electrical conductivity of potassium phosphate glasses containing Al_2O_3. *J. Non-Cryst. Solids* **2018**, *481*, 585–589. [CrossRef]
10. Khasa, S.; Dahiya, M.S.; Agarwal, A.; Chand, P. EPR, FTIR, thermal and electrical properties of VO^{2+} doped $BaCl_2{\cdot}BaO{\cdot}B_2O_3$ glasses. *J. Mol. Struct.* **2015**, *1079*, 15–20. [CrossRef]
11. Ramteke, D.; Swart, H.; Gedam, R. Electrochemical response of Nd^{3+} ions containing lithium borate glasses. *J. Rare Earths* **2017**, *35*, 480–484. [CrossRef]
12. Nakayama, S.; Watanabe, T.; Asahi, T.; Kiyono, H.; Aung, Y.L.; Sakamoto, M. Influence of rare earth additives and boron component on electrical conductivity of sodium rare earth borate glasses. *Ceram. Int.* **2010**, *36*, 2323–2327. [CrossRef]
13. Aung, Y.L.; Itani, K.; Asahi, T.; Kiyono, H.; Sakamoto, M.; Nakayama, S. Electrical properties of $(Na_2O)_{35.7}(RE_2O_3)_{7.2}(GeO_2)_{57.1}$ (RE = Sm, Gd, Dy, Y, Ho, Er and Yb) glasses. *Mater. Chem. Phys.* **2008**, *109*, 30–33. [CrossRef]
14. Vijay, R.; Babu, P.R.; Gandhi, Y.; Piasecki, M.; Rao, D.K.; Veeraiah, N.; Nalluri, V. Molybdenum ion: A structural probe in lithium–antimony–germanate glass system by means of dielectric and spectroscopic studies. *J. Mater. Sci.* **2014**, *49*, 6203–6216. [CrossRef]
15. El-Rabaie, S.; Taha, T.; Higazy, A. Non-linear optical and electrical properties of germanate glasses. *Phys. B Condens. Matter* **2013**, *429*, 1–5. [CrossRef]
16. Sklepić, K.; Banhatti, R.D.; Tricot, G.; Mošner, P.; Koudelka, L.; Moguš-Milanković, A. Insights from Local Network Structures and Localized Diffusion on the Ease of Lithium Ion Transport in Two Mixed Glass-Former Systems. *J. Phys. Chem. C* **2017**, *121*, 17641–17657. [CrossRef]
17. Braunger, M.L.; Escanhoela, C.A.; Fier, I.; Walmsley, L.; Ziemath, E.C. Electrical conductivity of silicate glasses with tetravalent cations substituting Si. *J. Non-Cryst. Solids* **2012**, *358*, 2855–2861. [CrossRef]
18. Wójcik, N.A.; Jonson, B.; Barczyński, R.J.; Kupracz, P.; Möncke, D.; Ali, S. Electrical properties of Na_2O-CaO-P_2O_5 glasses doped with SiO_2 and Si_3N_4. *Solid State Ion.* **2018**, *325*, 157–162. [CrossRef]
19. Wójcik, N.; Kupracz, P.; Barczyński, R.J.; Jonson, B.; Ali, S. Ion conduction in beryllium-alumino-silicate glasses doped with sodium or sodium and lithium ions. *Solid State Ion.* **2019**, *341*, 115055. [CrossRef]
20. Lee, W.; Cho, B.; Kang, B.; Kim, J.; Lee, J.; Jeong, C.; Kim, Y. Enhanced properties of ag alloy films for advanced TFT-LCD's. *J. Korean Phys. Soc.* **2002**, *40*, 110–114.
21. Levlin, M.; Laakso, A. Evaporation of silver thin films on mica. *Appl. Surf. Sci.* **2001**, *171*, 257–264. [CrossRef]
22. Seo, D.; Lee, J. Conductivity of silver paste prepared from nanoparticles. *Colloids Surf. A Physicochem. Eng. Asp.* **2008**, *313*, 351–354.
23. Majewski, A.J.; Dhir, A. Application of silver in microtubular solid oxide fuel cells. *Mater. Renew. Sustain. Energy* **2018**, *7*, 16. [CrossRef]
24. Kenmuir, S.V.J.; Thorp, J.S.; Kulesza, B.L.J. The dielectric behaviour of Mg-AI-Si, Ca-AI-Si, Y-AI-Si and Nd-AI-Si oxynitride glasses. *J. Mater. Sci.* **1983**, *18*, 1725–1730. [CrossRef]
25. Wójcik, N.; Kupracz, P.; Barczyński, R. Nonlinear electrical properties of glass-ceramics nanocomposites containing ferroelectric nanocrystallites of $Bi_2VO_{5.5}$. *Solid State Ion.* **2018**, *317*, 7–14. [CrossRef]
26. Szreder, N.A.; Kupracz, P.; Prześniak-Welenc, M.; Karczewski, J.; Gazda, M.; Barczyński, R.J. Nonlinear and linear impedance of bismuth vanadate ceramics and its relation to structural properties. *Solid State Ion.* **2015**, *271*, 86–90. [CrossRef]
27. Kupracz, P.; Karczewski, J.; Prześniak-Welenc, M.; Szreder, N.A.; Winiarski, M.J.; Klimczuk, T.; Barczyński, R.J. Microstructure and electrical properties of manganese borosilicate glasses. *J. Non-Cryst. Solids* **2015**, *423–424*, 68–75. [CrossRef]
28. Sołtys, M.; Górny, A.; Pisarska, J.; Pisarski, W.A. Electrical and optical properties of glasses and glass-ceramics. *J. Non-Cryst. Solids* **2018**, *498*, 352–363. [CrossRef]
29. Ný, J.; Al, D.; Kubliha, M.; Pedlíková, J.; Mariani, E. Electrical and dielectric properties of TeO_2-ZnO glasses. *Ceram. Silik.* **2002**, *46*, 140–147.
30. Kozioł, R.; Łapiński, M.; Syty, P.; Koszelow, D.; Sadowski, W.; Sienkiewicz, J.E.; Kościelska, B. Evolution of Ag nanostructures created from thin films: UV-vis absorption and its theoretical predictions. *Beilstein J. Nanotechnol.* **2020**, *11*, 494–507. [CrossRef]
31. Thompson, C.V. Solid-State Dewetting of Thin Films. *Annu. Rev. Mater. Sci.* **2012**, *42*, 399–434. [CrossRef]
32. Garcia, M.A. Surface plasmons in metallic nanoparticles: Fundamentals and applications. *J. Phys. D Appl. Phys.* **2011**, *44*, 283001. [CrossRef]

33. Gromov, D.; Gavrilov, S.; Redichev, E.N.; Dubkov, S. Melting and dissociation of thin Au films into droplets on the inert Al_2O_3 surface under thermal treatment. *Trends Phys. Chem.* **2015**, *14*, 45–51.
34. Wójcik, N.; Ali, S.; Möncke, D.; Tagiara, N.; Kamitsos, E.; Segawa, H.; Eriksson, M.; Jonson, B. The influence of Be addition on the structure and thermal properties of alkali-silicate glasses. *J. Non-Cryst. Solids* **2019**, *521*, 119532. [CrossRef]
35. Wójcik, N.A.; Ali, S.; Karczewski, J.L.; Jonson, B.; Bartmański, M.; Barczyński, R.J. DC and AC Conductivity, Biosolubility and Thermal Properties of Mg-Doped Na_2O–CaO–P_2O_5 Glasses. *Materials* **2021**, *14*, 2626. [CrossRef]
36. Jonscher, A.K. Universal Dielectric Response. *Nature* **1977**, *267*, 673–679. [CrossRef]
37. Macdonald, J. *Impedance Spectroscopy: Emphasizing Solid Materials and Systems*; John Wiley & Sons Inc.: Hoboken, NJ, USA, 1989.
38. Fan, J.; Tan, C.S. Metallurgy—Advances in Materials and Processes. In *Low Temperature Wafer-Level Metal Thermo-Compression Bonding Technology for 3D Integration*; Pardhi, Y., Ed.; IntechOpen: New York, NY, USA, 2012; pp. 71–94.
39. Lani, S.; Bosseboeuf, A.; Belier, B.; Clerc, C.; Gousset, C.; Aubert, J. Gold metallizations for eutectic bonding of silicon wafers. *Microsyst. Technol.* **2006**, *12*, 1021–1025. [CrossRef]